Journal of the Brazilian Society of Mechanical Sciences and Engineering (2019) 41:387
https://doi.org/10.1007/s40430-019-1890-9

TECHNICAL PAPER

Effect of inertia on the cavitation phenomena of hydrodynamic textured bearings considering slip

J. Jamari[1] · M. Muchammad[2] · F. Hilmy[1] · M. Tauviqirrahman[1]

Received: 15 May 2019 / Accepted: 26 August 2019

Abstract

Surface modification of a lubricated bearing, such as hydrophobic coating inducing slip situation and texturing, is proved to enhance hydrodynamic performance. As widely known, in textured surface lubricant inertia and cavitation can significantly affect the hydrodynamic pressure profile. However, a brief literature review indicates that studies related to the correlation between cavitation and inertia, especially in the presence of slip, are considerably limited. The present study examines the effect of inertia on cavitation phenomena by considering the slip boundary using two approaches, namely computational fluid dynamics based on full Navier–Stokes equations and analytical lubrication equation based on the Reynolds equation. The modified Reynolds equation with slip concept is used with respect to the slip effect applied on the surface of the bearing. The results indicate that the inertia as well as the slip condition significantly affects the cavitation area. It is also highlighted that the cavitation area reduces by increasing the inertia effect, and it becomes smaller when the slip is introduced.

Keywords Cavitation · Computational fluid dynamics (CFD) · Inertia · Lubrication · Slip

List of symbols

a	Inlet length
b	Texture (dimple) length
B_o	Slider length
c	Outlet land length
h_d	Texture depth
h_o	Land film thickness in inlet land at B
p_atm	Atmospheric pressure
p_cav	Cavitation pressure
U	Sliding velocity
W	Load support
x	Coordinate in sliding direction
z	Coordinate through film thickness
μ	Lubricant dynamic viscosity
α_s, α_h	Slip coefficients at surface s (moving) and h (stationary)

1 Introduction

Surface texturing is an effective technique to enhance the tribological performance of lubricated mechanical components. As widely known, the introduction of textured surfaces can significantly affect the load support of sliding bearings. Recently, significant efforts have been focused on investigating the influence of the geometric parameters of texture. When texture is applied on the bearing, inertia and cavitation may exist and affect the lubrication performance.

Several studies reported that the inertia significantly affects bearing performance both theoretically [1–7] and numerically [8–10]. Based on analytical approach, Safar and Shawki [1] investigated the effect of inertia force on the turbulent bearing characteristics. The results revealed that the consideration of inertia effects leads to increased pressure. The effect appears considerably insignificant albeit favourable. The finding was also strengthened by the results of a study by Kakoty and Majumdar [2]. They concluded that the steady-state characteristic of bearing is not significantly affected by fluid inertia. However, its effect cannot

Technical Editor: Daniel Onofre de Almeida Cruz, D.Sc.

✉ M. Tauviqirrahman
mtauviq99@yahoo.com

[1] Laboratory for Engineering Design and Tribology, Mechanical Engineering Department, Faculty of Engineering, University of Diponegoro, Jl. Prof. Soedarto, SH, Tembalang, Semarang 50275, Indonesia

[2] Laboratory for Surface Technology and Tribology, Faculty of Engineering Technology, University of Twente, Drienerloolan 5, Postbox 217, 7500 AE Enschede, The Netherlands

Published online: 03 September 2019

be ignored. Khalil et al. [3] performed a theoretical analysis and stated that the convective inertia force combined with centrifugal force increases the pressure inside the recess and land regions. However, in squeeze film air contact, the results indicated that fluid inertia does not significantly affect the load-carrying capacity of the contact [4]. Syed and Sarangi [8] examined the lubricating performance of textured parallel sliding contacts considering fluid inertia effect. The results indicated that fluid inertia effect leads to changes in the performance parameters. Woloszynski et al. [9] evaluated the inertia effect in finite hydrodynamic bearings with surface texturing using a spectral element solver. They concluded the inertia effect increases with increasing Reynolds number and decreasing dimple aspect ratio (i.e. ratio of dimple length to dimple depth). The result was also consistent with the study of Dobrica and Fillon [10]. Specifically, they conducted a parametric study on the texturing parameters, dimension (depth and width), number, and density of the cells to improve hydrodynamic performance. They analysed the validity of the Reynolds equation (RE) and inertia effects in parallel textured sliders of infinite width using the RE and commercial CFD simulation software (FLUENT). In the case of journal bearing, the longitudinal inertia has a dominant influence on the increase in the values of the bearing mechanical parameters, while the circumferential inertia causes a small decrease in the pressure and load-carrying capacity [5]. In a recent study, Okabe [6] revealed that the fluid inertia generates more hydrodynamic load although it does not significantly alter bearing stiffness or damping.

It should be noted that most of the aforementioned studies focused on the inertia effect in the analysis of bearing lubrication. As widely known, when the texturing is of specific interest, the presence of cavitation can reduce or increase the lubrication performance based on the texturing parameters. In terms of inertia and cavitation, in the recent publication, Lin et al. [7] discussed the complete analysis of the thermohydrodynamic cavitating flow lubrication model including effects of cavitation, inertia, and turbulence. The results indicated that inertia and cavitation reduce the load-carrying capacity and friction torque, while load-carrying capacity and friction torque increase due to turbulence. Another interesting result was that the influence of inertia effect on the static characteristics of bearing exceeds the cavitation effect under a high-speed condition.

In addition to surface texturing, the slip induced by hydrophobic coating is considered as a technique to enhance lubrication performance. Several researchers including Salant and Fortier [11], Wu et al. [12], Ma et al. [13, 14], Bayada and Meurisse [15], Rao [16], Aurelian et al. [17], Tauviqirrahman et al. [18], Syed and Sarangi [19], and Wang and Lu [20] explored the behaviour of the sliding contact with respect to the effect of slip on the load support and friction. The results indicated the existence of a lift force (load support) even in the absence of a wedge effect. It should be noted that most of the studies ignored the presence of the cavitation.

The literature survey shows that the studies related to the correlation between cavitation and inertia and especially in the presence of the slip are significantly limited. The present study focuses on predicting the hydrodynamic pressure via computational fluid dynamic (CFD) and modified Reynolds equation to explore the influence of inertia and slip boundary on the hydrodynamic pressure of textured parallel sliding contacts by considering cavitation. In this research, an analytical model of the RE considering cavitation based on a study by Muchammad et al. [21] is adopted.

2 Methodology and its solution

2.1 Geometric model

The textured bearing configuration is shown in Fig. 1. The textured surface is composed of a single recess with or without boundary slip. For the analysis of a pocketed bearing with slip condition, the boundary slip is engineered to occur on the complete stationary surface and all sides of the pocket cell (see Fig. 1) as denoted by the red line with circles. For all the following simulations, the standard one-dimensional bearing geometry is investigated with values

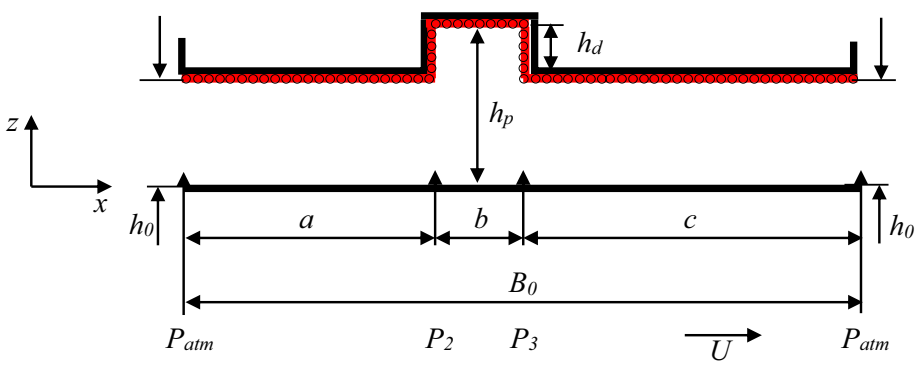

Fig. 1 Schematic diagram of parallel textured bearing with boundary slip

for the parameter as shown in Table 1. It should be noted that the parameters employed in this study are inspired by the works of Muchammad et al. [21], Olver et al. [22], and Fowell et al. [23].

In the present study, to explore the correlation between the inertia, the cavitation, and the slip, two cases varying different geometric textures are of main particular interest. Case 1 refers to the bearing with texture depth h_d of 2 μm (i.e. $h_d = 0.5\ h_o$), and case 2 refers to the one with h_d of 4 μm (i.e. $h_d = h_o$). For each case, the texture length b is varied to 0.25 mm and 0.75 mm as shown in Fig. 2. According to Dobrica and Fillon [10], in this way the inertia effect as a function of texture depth as well as texture length can be evaluated in terms of the hydrodynamic pressure. For all cases, Reynolds number is set to be constant, i.e. 0.286. In the present analysis, when slip is of particular interest, the slip condition is implemented to all stationary surfaces including the texture cell as mentioned before. It should be noted that the inlet length a is set to constant, i.e. 0.75 mm. Consequently, when the b value is varied, the outlet length c will change.

Table 1 Characteristics of the analysed main bearing

Parameter	Symbol	Value	Unit
Length of the bearing	B	2.00	mm
Inlet length	a	0.75	mm
Length of texture	b	0.25 and 0.75	mm
Outlet length	c	1.00 and 0.50	mm
Land film thickness	h_o	4.00	μm
Texture depth	h_d	2.00 and 4.00	μm
Density of oil	ρ	962	kg/m^3
Density of vapour	ρ_v	0.02556	kg/m^3
Viscosity of oil	μ	0.013468	Pa s
Viscosity of vapour	μ_v	1.256×10^{-5}	Pa s
Atmospheric pressure	p_{atm}	100	kPa
Cavitation pressure	p_{cav}	50	kPa
Slip coefficient	α	0.02	m^2 s/kg
Sliding velocity	u	1	m/s

2.2 Governing equations

In the present study, the analysis of lubrication is solved by two methods as follows: an analytical solution based on modified Reynolds theory with slip and a more rigorous computational fluid dynamics method based on Navier–Stokes (N–S) equations. For the first approach, the lubrication theory is modified by including slip and cavitation based on the derivation of first-order Reynolds theory. The analytical mathematical lubrication equation used in the analysis is as follows [21]:

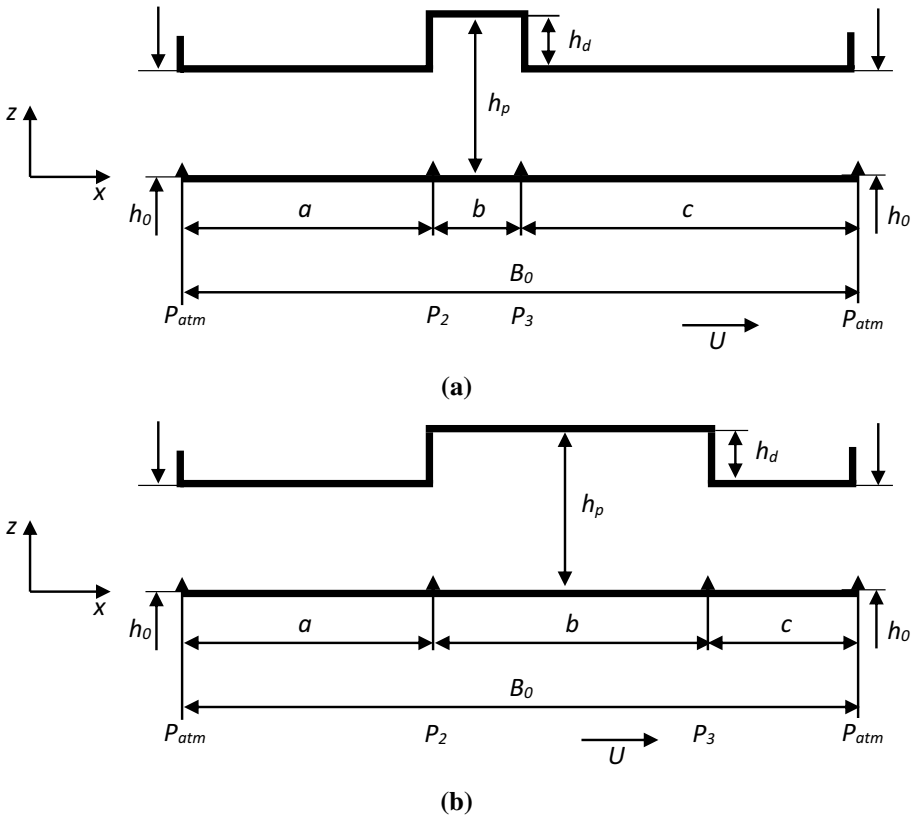

Fig. 2 Schematic representation of the textured slider bearing for the case of **a** low b (i.e. $b = 0.25$ mm) and **b** high b (i.e. $b = 0.75$ mm)

$$P_2\left[\left(h_p^3+3h_p^3K_p\right)\frac{ab+bc}{ab^2}+\left(\frac{h_o^3+3h_o^3K_o}{a}\right)\right]=P_{\text{atm}}\left[\left(h_p^3+3h_p^3K_p\right)\frac{ab+bc}{ab^2}+\left(\frac{h_o^3+3h_o^3K_o}{a}\right)\right]-6\mu U\left[\left(h_p+h_pK_p\right)-\left(h_o+h_oK_o\right)\right] \quad (1)$$

The detailed solution method used in this research is presented in "Appendix". The reader can also refer to the published work of Muchammad et al. [21] for detailed algorithm used.

For the second method, the Navier–Stokes (N–S) equations are solved over the domain using a finite volume method with the commercial CFD software package FLUENT®. The equations are applied with constant density and viscosity and without body force. The equations are steady and only solved in the x- and z-directions. Given the aforementioned properties, the Navier–Stokes and continuity equations are, respectively, expressed as follows:

$$\rho(\mathbf{u}\cdot\nabla)\mathbf{u}=-\nabla p+\eta\nabla^2\mathbf{u} \quad (2)$$

$$\nabla\cdot\mathbf{u}=0 \quad (3)$$

With the application of sliding surfaces in very narrow-gap conditions and the availability of hydrophobic materials, the classical no-slippage boundary condition breaks down. When lubricant slips along a solid–liquid interface, the slippage length β is generally used to address the relation between slippage velocity and surface shear rate as follows:

$$u_{\text{s}}=\beta\left.\frac{\partial u}{\partial z}\right|_{\text{surface}} \quad (4)$$

where u_{s} denotes the streamwise slippage velocity at the hydrophobic surface, β denotes the slippage length, and $\partial u/\partial z|_{\text{surface}}$ denotes the surface shear rate. Typically, it is postulated that a high value of β implies greater slippage. Furthermore, it is also conventionally implied that the high slippage is also associated with high friction force reduction. Numerous studies demonstrated that the chemical treatment of the surface generates a slippage length in the order of 1 µm, whereas longer slippage lengths of up to 100 µm are obtained through combinations of deterministic textured structures with hydrophobic surfaces. In the present study, the slippage length of a hydrophobic surface is assumed as uniform in space due to the application of a microscopic scale.

To model the Navier slippage behaviour in ANSYS-FLUENT, it is a necessary to create an additional subroutine to enhance the capability of FLUENT and customise its feature for a lubrication modelling analysis. This subroutine, termed as user-defined function (UDF), is a function that allows a user to define boundary conditions, material properties, and source terms for the flow regime as well as specify customised model parameters. Thus, the Navier slippage boundary condition can be applied to surfaces of the lubricated sliding contact.

The flow is considered turbulent to ensure that the conditions are representative of the bearing characteristics. The turbulent model of Realisable k–ε is used with standard wall functions as near-wall treatment. In FLUENT®, three cavitation models are available as follows: the Schneer and Sauer model, Zwart–Gerber–Belamri model, and Sighal et al. model [24]. In this study, the Zwart–Gerber–Belamri model is employed owing to its capabilities such as less sensitivity to mesh density, robustness, and quick convergence [24].

In cavitation, the liquid–vapour mass transfer (evaporation and condensation) is governed by the vapour transport equation as follows [24]:

$$\frac{\partial}{\partial t}\left(\alpha_{\text{v}}\rho_{\text{v}}\right)+\nabla.\left(\alpha_{\text{v}}\rho_{\text{v}}v\right)=R_g-R_c \quad (5)$$

where α_{v} denotes the vapour volume fraction and ρ_{v} denotes the vapour density. Additionally, R_g and R_c account for the mass transfer between the liquid and vapour phases in cavitation. For the Zwart–Gerber–Belamri model, the final form of the cavitation is as follows:

$$\text{If}\quad p\le p_{\text{v}},\quad R_g=F_{\text{evap}}\frac{3\alpha_{\text{nuc}}\left(1-\alpha_v\right)\rho_v}{R_{\text{B}}}\sqrt{\frac{2}{3}\frac{P_v-P}{\rho_{\text{l}}}} \quad (6)$$

$$\text{If}\quad p\ge p_{\text{v}},\quad R_c=F_{\text{cond}}\frac{3\alpha_v\rho_v}{R_{\text{B}}}\sqrt{\frac{2}{3}\frac{P-P_v}{\rho_{\text{l}}}} \quad (7)$$

where $F_{\text{evap}}=$ evaporation coefficient $=50$, $F_{\text{cond}}=$ condensation coefficient $=0.01$, $R_{\text{B}}=$ bubble radius $=10^{-6}$ m, $\alpha_{\text{nuc}}=$ nucleation site volume fraction $=5\times10^{-4}$, $\rho_{\text{l}}=$ liquid density, and $p_{\text{v}}=$ vapour pressure.

2.3 Boundary condition and computational mesh analysis

The flow is assumed to be incompressible, steady, and the Newtonian fluid. In the current study, the boundary slip is applied on the entire surface of stationary wall including the edges of texture), while the no-slip boundary condition is applied on the moving wall. In detail, the boundary condition of the domain is shown in Fig. 3. At the inlet and outlet of the domain, the pressure is set to atmospheric and a zero velocity gradient in the direction normal to sliding is

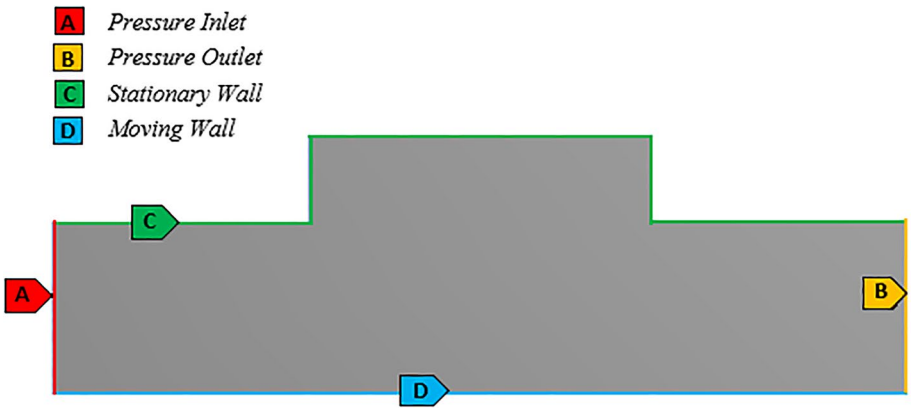

Fig. 3 Boundary condition of the computational domain

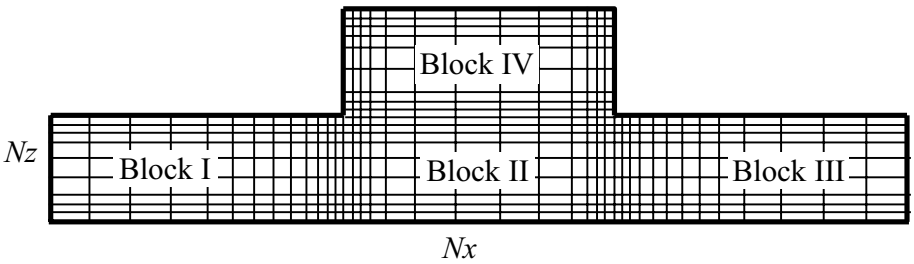

Fig. 4 Mesh structure of the computational domain

assumed. This can also be thought of as a fully developed flow approximation. Additionally, to investigate the cavitation effect, the comparison of the lubrication performance between the analysis with cavitation model and that without cavitation model is also discussed.

In the CFD approach, meshing of the computational domain is needed in order to solve the continuity and momentum equations over each grid cell. The high-resolution scheme in FLUENT is used to discretise. It should be noted that the meshing process for the textured surfaces has been checked to ensure grid independent result. Thus, to evaluate the necessary mesh density for determining the lubricant behaviour of bearing accurately, a mesh analysis was conducted. In the computational domain, the developed mesh consists of four blocks with uniform grid as shown in Fig. 4. The minimum mesh size in the longitudinal (Nx) and transverse (Nz) directions is 1000×140, respectively. In the textured area, a finer mesh is used. The mesh density is in detail shown in Table 2.

Table 2 Detail of mesh used

No.	Blok		Mesh edge type	Ratio	Interval count
1	I	NX	First last ratio	0.1	375
		NZ	Bi-exponent	0.6	60
2	II	NX	Bi-exponent	0.6	250
		NZ	Bi-exponent	0.6	60
3	III	NX	Last first ratio	0.6	375
		NZ	Bi-exponent	0.6	60
4	IV	NX	Bi-exponent	0.6	40; 80; 160
		NZ	Bi-exponent	0.6	125; 250; 500

3 Results

3.1 Validation

In this subsection, the developed methods in the present work (i.e. N–S and RE approaches) are validated by comparing the computed hydrodynamic pressure with those of Ref. [22] under the same input parameters. It should be noted that the validity of mass preserving multi-phase cavitation model used in the CFD approach is also of particular interest. As shown in Fig. 5, the hydrodynamic pressures predicted by the present study by either CFD or Reynolds approaches are in good agreement with the corresponding results in Ref. [22], which justify the validation of the developed bearing model. The cavitation region predicted by two approaches employed here (based on N–S and RE) also matches well with the reference. However, as shown in insert in Fig. 5, there is an acceptable small difference with respect to the pressure peak as well as the cavitation region. The reason behind this is that, first, CFD method solves the Navier–Stokes equation in which the inertia term is included; second, the CFD approach employs the multi-phase cavitation model instead of single-phase model to model the cavitation phenomena. The validity of the multi-phase cavitation model as used here

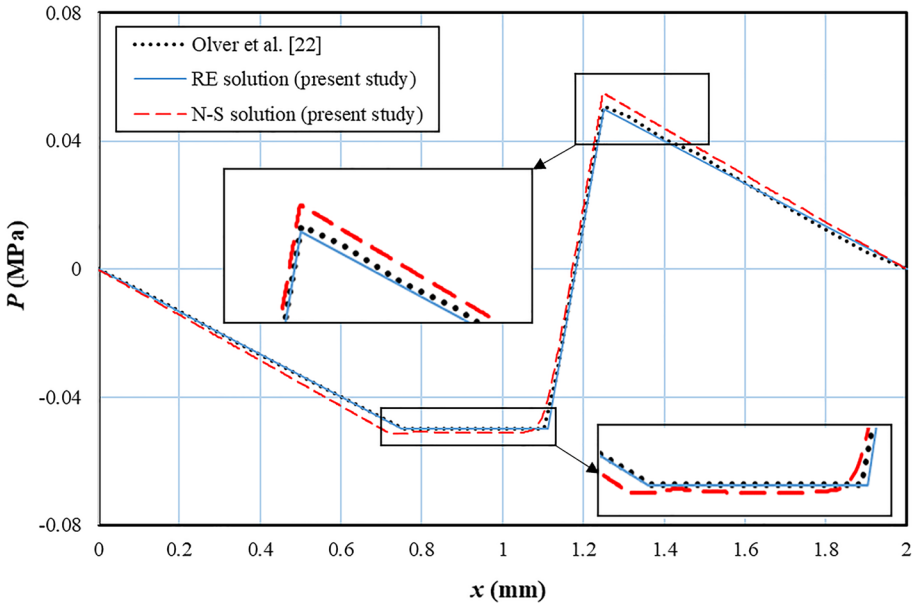

Fig. 5 Comparison of pressure between the present study and the literature

has been discussed in detail in the recent literatures [25, 26]. In what follows, all numerical computations are performed based on the present solution set-up.

3.2 Effect of inertia

According to Dobrica and Fillon [10], the inertia effect can be determined by the Reynolds number *Re* and/or texture aspect ratio λ (i.e. $\lambda = b/h_d$). In this section, the textured bearing configurations are classified into two cases varying the textured depths, i.e. case 1 ($h_d = 0.5h_o$) and case 2 ($h_d = h_o$). For case 1, the resulted texture aspect ratios λ are 125 and 375, respectively, for case of texture length $b = 0.25$ mm and $b = 0.75$ mm. For case 2, the λ are 62.5 and 187.5, respectively, for case of $b = 0.25$ mm and $b = 0.75$ mm. Based on "inertia" mapping presented by Dobrica and Fillon [10], assuming the same Reynolds number (i.e. $Re = 0.28$ in this study), the textured bearing in case 2 has more inertia effect than that in case 1, which means that the variations in film thickness with respect to the texture depth are larger. Additionally, for each case the variation of texture length *b* is conducted to provoke the inertia effect. Physically, lowering the value of *b* (i.e. 0.25 mm) of the textured bearing will generate more inertia effect in comparison with the bearing with high *b* (i.e. 0.75 mm).

Case 1 In this section, the textured bearings with $h_d = 0.5\ h_o$ is of particular interest. Based on Fig. 6a, for the no-slip situation and low *b*, it is observed that the hydrodynamic pressure profiles predicted by the Navier–Stokes equation (N–S) and the Reynolds equation (RE) are identical for the case in which the cavitation effect is ignored. However, when the cavitation model is considered, the pressure distribution predicted by the N–S exceeds that by the RE and especially in the centre of the contact. Based on a physical view point, this means that inertia with the presence of the cavitation increases the hydrodynamic pressure. Another interesting result is shown in Fig. 6b with respect to the bearing pattern with high *b* wherein the RE yields a slight deviation of the pressure prediction with respect to the N–S and especially in the outlet edge of the contact. For the case of "no cavitation" predicted by both the N–S and the RE, the prediction of the hydrodynamic pressure profiles yields the same result. Overall, there are two specific features specified based on Fig. 6. First, for low *b*, inertia plays a significantly strong dominant role in altering the flow behaviour in terms of hydrodynamic pressure. Second, for high *b*, the inertia effect is not significant. However, in the case of "high *b*", the cavitation effect becomes dominant. In other words, the results indicate that presence of the inertia decreases the possibility of the occurrence of cavitation as shown clearly in Fig. 6a.

For the slip situation shown in Fig. 7, some specific features are highlighted. First, the predictions of the hydrodynamic pressure profiles between "cavitation" and "no-cavitation" cases tend to coincide with each other. This prevails for the pressure distribution predicted by both the N–S and RE. It indicates that for the case in which the inertia is dominant (i.e. low *b*), the presence of cavitation is significantly reduced by introducing the slip. This is different when the no-slip is employed as reflected in Fig. 6a. Second, in the case in which the inertia is less dominant (i.e. high *b*), it is observed based on Fig. 7b that the prediction of the pressure between the N–S and the RE coincides irrespective of the cavitation model. This is as expected because the inertia is less significant in the bearing with

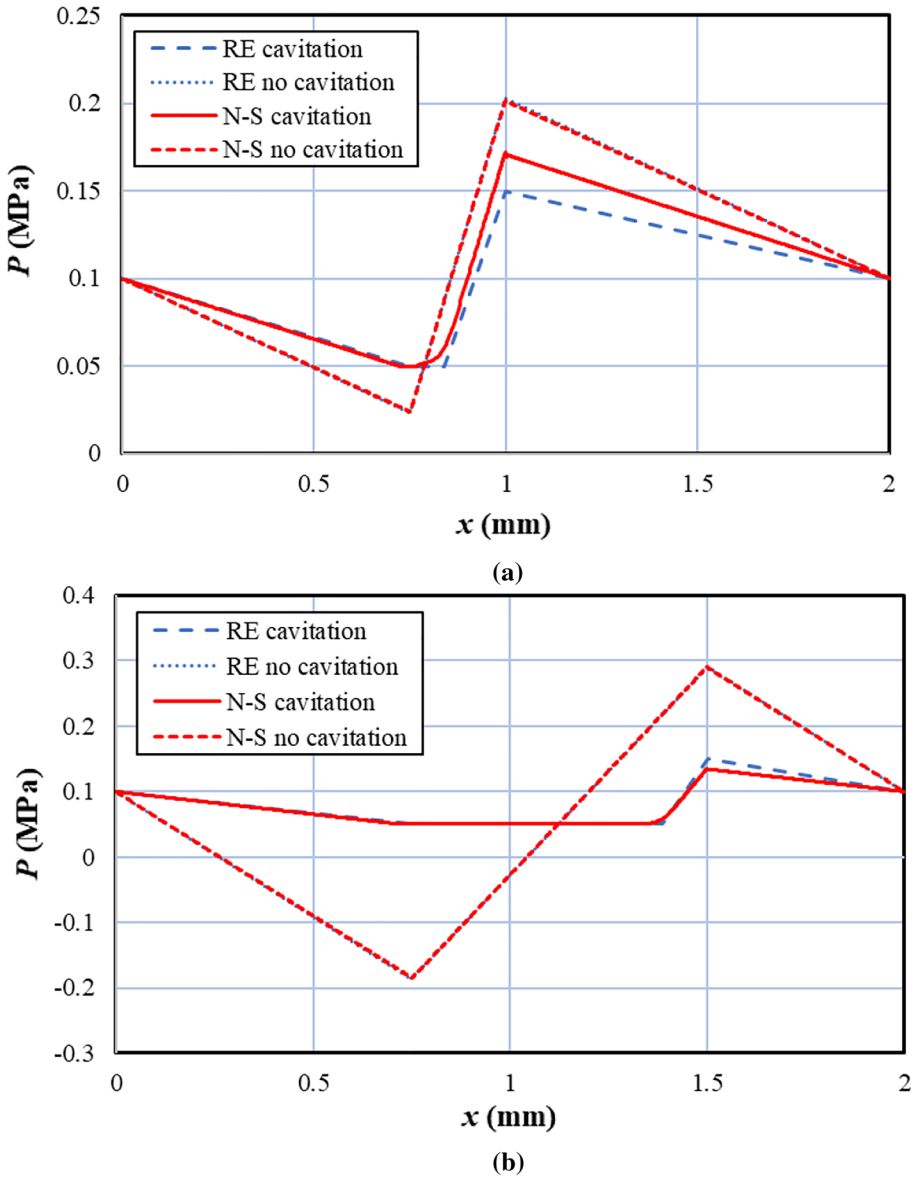

Fig. 6 Hydrodynamic pressure for the no-slip situation in the case of **a** low b and **b** high b

high b. However, while dealing with the cavitation effect, the prediction is considerably different with respect to the prediction of the pressure when the cavitation model is not considered when the case is solved by the N–S as well as when it is solved by the RE. This indicates that inertia and the cavitation exhibit a strong relation irrespective of the slip being introduced (see Fig. 4b). It is observed that the increase in the inertia effect (i.e. by lowering the value of b in this case) will decelerate the cavitation phenomena. Figure 7a strengthens the results shown in Fig. 6a.

With respect to the N–S solution in which the inertia effect is considered, based on Figs. 6 and 7, it is found that for the no-slip case, the consideration of the cavitation model in the computation makes the numerical results more realistic by the presence of the cavitation area in texture. The "no-cavitation" approach yields the "overestimation" results. Nevertheless, when the slip condition is introduced, the lines of pressure profiles coincide, and this means that the slip minimises the presence of cavitation. Based on Figs. 6b and 7b, for the case of bearing with high b (i.e. low inertia), it is observed that the cavitation region is minimised by introducing the slip situation. Additionally, for the "no-cavitation" case, the introduction of the slip yields a lower prediction of the pressure when compared to that in the "no-slip" case.

For the numerical results based on RE (i.e. inertia terms is excluded) dealing with the case of low dimple length b, based on Figs. 6a and 7a, it can be seen that for the slip condition, there is no difference between the "cavitation" and the "no-cavitation" approaches. This is quite similar to the case when the N–S is used. The difference is that the N–S represents what the so-called pressure jump as found in the texture edges. The reason behind this is that the

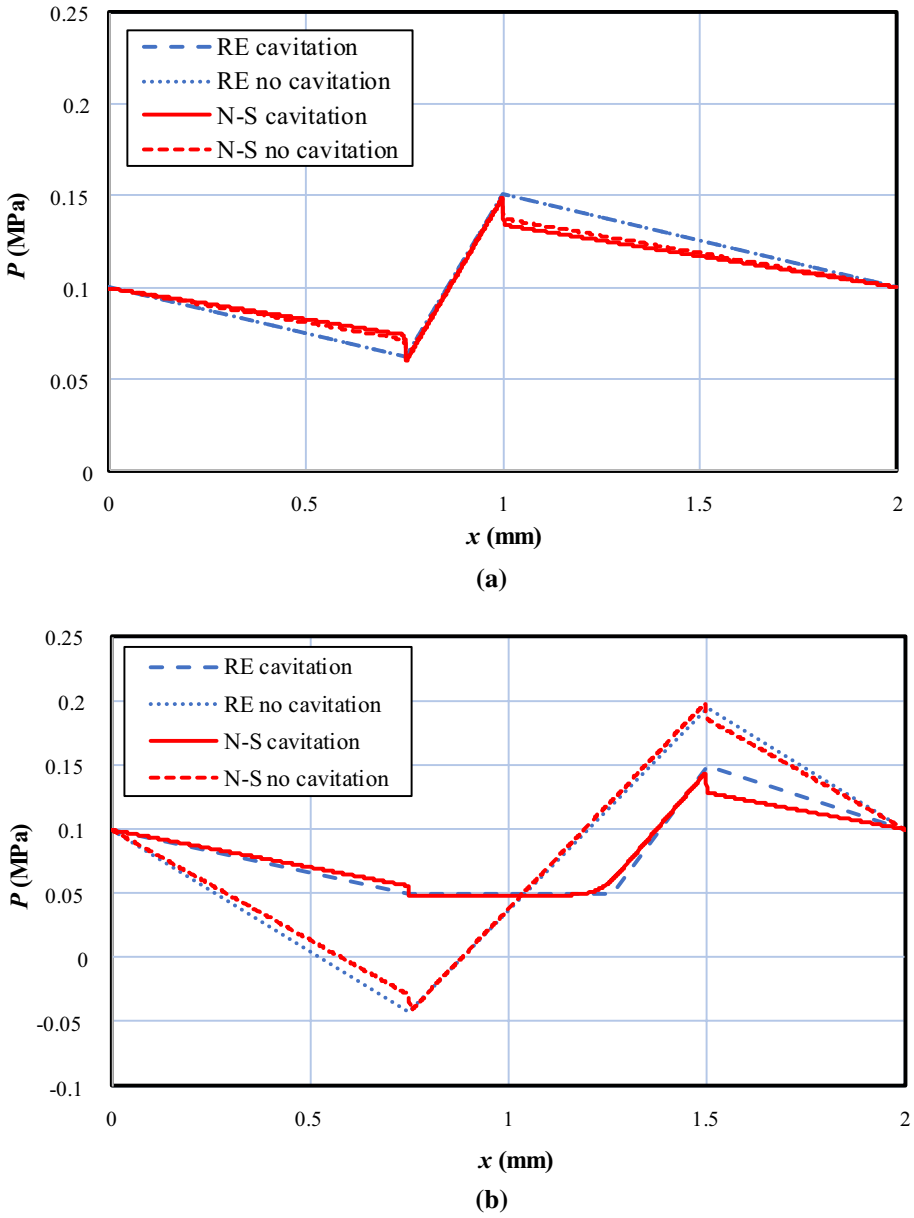

Fig. 7 Hydrodynamic pressure for the slip situation in the case of **a** low b and **b** high b

inertia alters the flow in that area. The interesting finding based on Figs. 6a and 7a is the fact that the cavitation does not occur for slip situation. It means that slip can minimise the existence of cavitation. For the no-slip case, as expected, the cavitation approach makes the profiles lower than the "no-cavitation" approach. Again, these results are similar to the results predicted by N–S approach.

Regarding the cases of textured bearing with high b, based on Figs. 6b and 7b, it is found that the pressure profiles predicted by the RE are very similar to that solved by the N–S. This is as expected because for the bearing with high b, the low inertia is found. Dealing with inertia effect, comparing Figs. 6 and 7, the cavitation region is found to be larger in bearing with low inertia (i.e. high b) in comparison with the bearing with low b. This is to say that the inertia as well as slip boundary can reduce the presence of cavitation in bearing.

Case 2 In this part, the textured bearings with $h_d = h_o$ are of particular interest. As mentioned earlier, increasing the texture depth h_d while keeping the land film thickness h_o constant makes the inertia more significant [10]. Therefore, the main focus in this section is that in the presence of inertia, the correlation between the slip and the cavitation is investigated.

Figure 8 shows the Navier–Stokes prediction of the hydrodynamic distribution pressure varying the texture length for slip and no-slip situations. It can be seen that there are some interesting features which can be drawn.

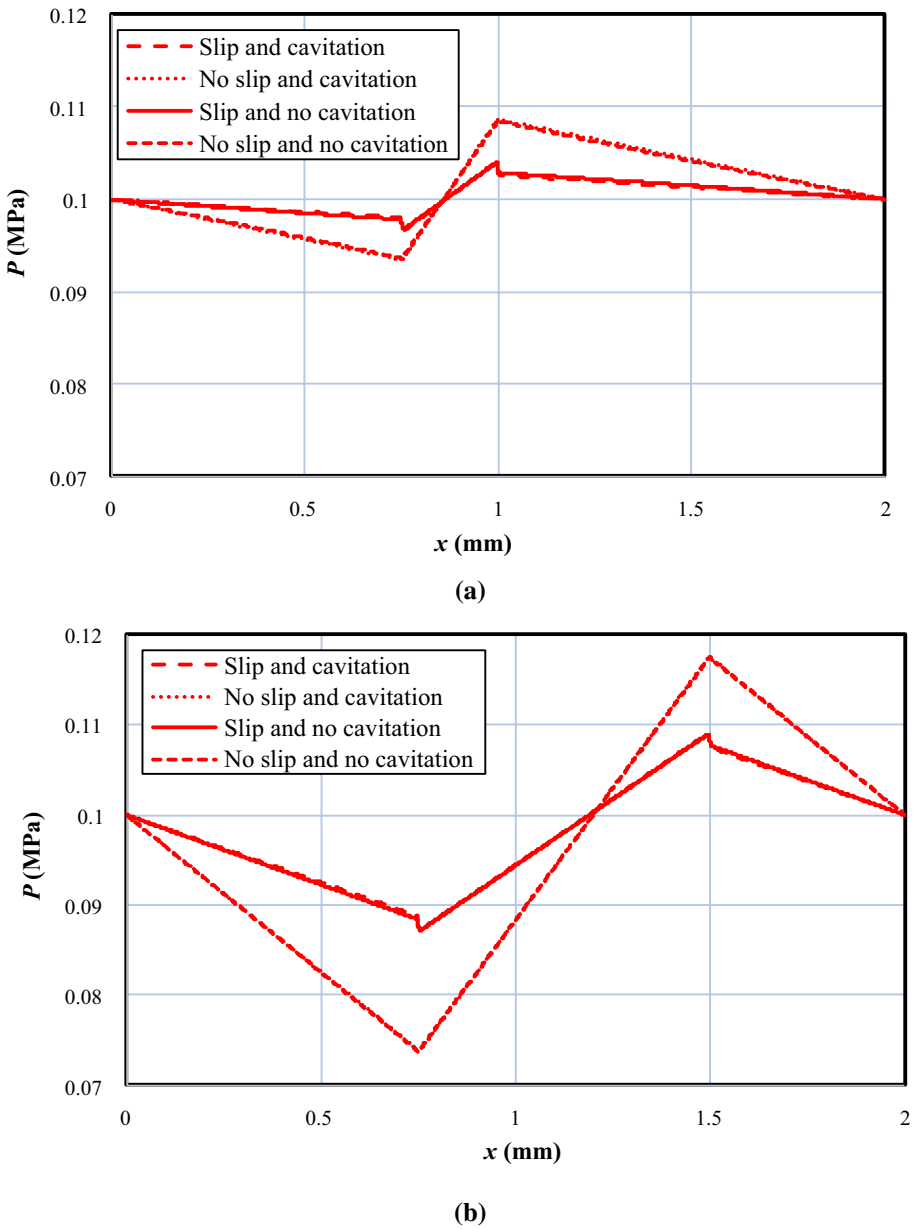

Fig. 8 Pressure distribution predicted by Navier–Stokes solution in the case of **a** low *b* and **b** high b

First, for all situations (i.e. slip and no-slip), the cavitation phenomena are not found. The predicted results without considering the cavitation model also give the same trends. Generally speaking, for the bearing with significant inertia effect, the cavitation can be prevented. This result, of course, strengthens the previous results of case 1 dealing with the presence of inertia. Second, dealing with slip effect, it is found that the slip reduces the hydrodynamic pressure profile irrespective of the value of *b*. However, other interesting finding is the fact that when the inertia effect is reduced by increasing the *b*, the deviation of the pressure profile between the "slip" analysis and the "no-slip" analysis becomes larger compared to the bearing with low *b*. It indicates that the slip effect becomes more dominant to alter the hydrodynamic pressure profile when the inertia effect is reduced. In other words, the presence of the inertia in textured bearing reduces the effect of the slip application.

4 Discussion

In the present work, the inertia effect is investigated by comparing the solution results of N–S and RE. If the deviation of the prediction is found, the inertia effect is highlighted. Figure 9 shows the prediction of hydrodynamic

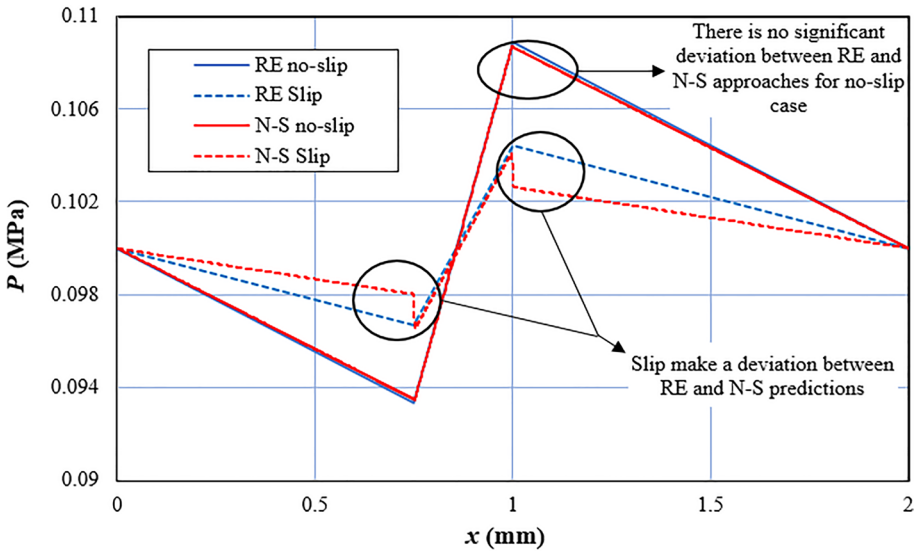

Fig. 9 Prediction of hydrodynamic pressure by Navier–Stokes and Reynolds equations for slip and no-slip situations considering cavitation

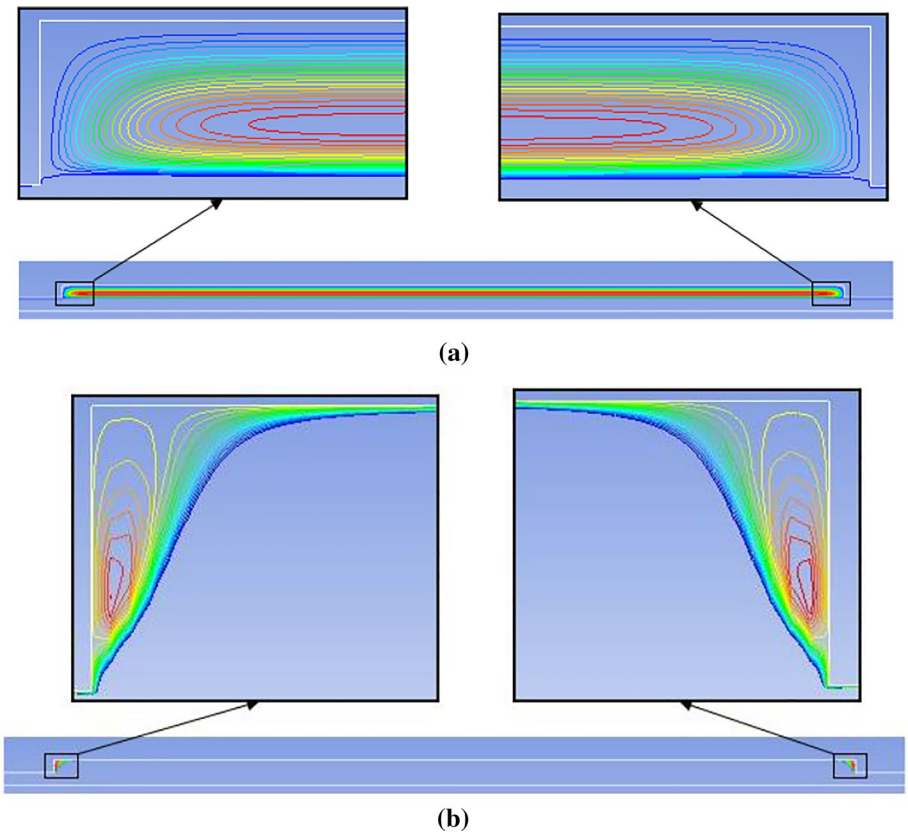

Fig. 10 Streamline of textured bearing for the case of **a** no-slip and **b** slip conditions. *Note*: Results are evaluated by considering the cavitation model

pressure by N–S and RE approaches with the inclusion of the cavitation effect for slip and no-slip situations. It can be revealed that for the case of slip situation, the deviation between the Navier–Stokes and Reynolds equations is observed. Based on the physical point of view, it means that the slip condition generates a special phenomenon in the edges of the texture cell as shown in Fig. 9. To explain what phenomenon is created by applying the slip situation, Fig. 10 reflects the streamline in texture cell for no-slip and slip conditions, respectively. As shown in Fig. 10a for case of no-slip, the vortex does not develop in the edge of the texture, while for slip textured bearing, Fig. 10b shows that the vortex occurs in the edge of the texture (front and rear). It means that the inertia effect becomes clearer when the slip is employed. Based on the CFD solution by considering the multi-phase

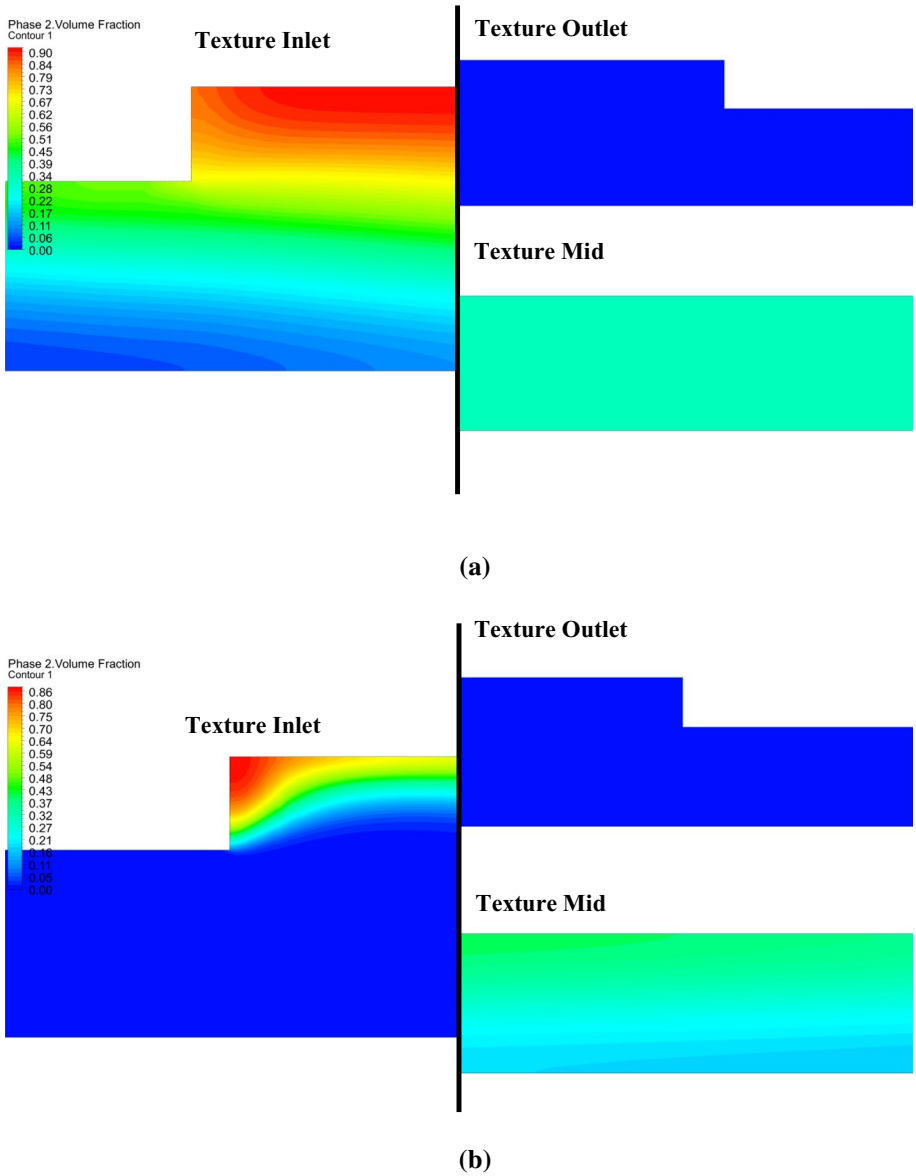

Fig. 11 Contour of volume fraction of vapour for the case of **a** no-slip and **b** slip conditions

cavitation model dealing with the question of "how the inertia affects the cavitation region", Fig. 11 shows the contour of volume fraction of vapour around the texture cell for no-slip and slip conditions. Comparing Figs. 10b and 11b, it is clear that in the leading edge of the texture cell, the volume of the vapour in the case of slip condition is lesser than that in the case of no-slip due to the presence of the more vortex. It is interesting to summarise the tribological performance in terms of load support for several conditions as shown in Fig. 12. Figure 12 depicts the comparison of the load support between the "low-inertia" bearing (i.e. $\lambda = 375$) and "high-inertia" bearing (i.e. $\lambda = 62.5$) for no-slip situation. It can be observed that the increase in the inertia effect increases the load support. This is as expected because as mentioned in the

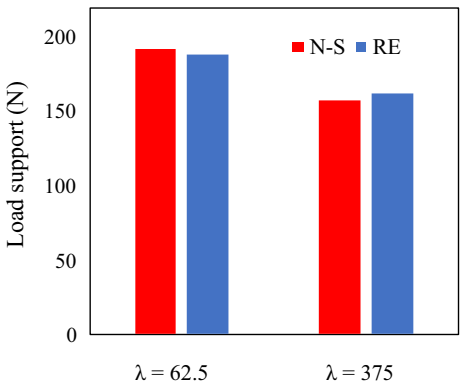

Fig. 12 Comparison of load support W for several conditions

previous discussion, due to the presence of inertia, the cavitation region also reduces.

5 Conclusion

This study focused on exploring the correlation between inertia, slip, and cavitation in a bearing. Two approaches were used to solve the problem, namely the CFD and modified RE with slip. The following conclusions were obtained in the present study:

1. The inertia effect significantly affects the cavitation. The presence of the inertia in textured bearing decelerates the cavitation phenomena.
2. The slip boundary reduces the cavitation area in the bearing.
3. In the case of "low-inertia" bearing, the slip effect becomes more dominant in altering the hydrodynamic pressure profiles compared to the case of "high-inertia" one.

Appendix

The analysis below is based on continuity of flow through the bearing. For the condition in which the slip velocity is present on the stationary surface, the corresponding flow rate equation can be expressed as [21]:

$$q_x = -\frac{\partial}{\partial x}\left(\frac{h^3}{12\mu}\frac{\partial p}{\partial x}\frac{h^2+4\mu h\alpha_h}{h(h+\mu\alpha_h)}\right)+\frac{U}{2}\frac{\partial}{\partial x}\left(\frac{h^2+2\mu h\alpha_h}{2(h+\mu\alpha_h)}\right) \tag{8}$$

For the first-order Reynolds equation, the flow rate is given:

$$q_x = \frac{U}{2}\frac{h^2+2\mu h\alpha_h}{h+\mu\alpha_h}-\frac{h^3}{12\mu}\frac{h+4\mu\alpha_h}{h+\mu\alpha_h}\frac{\mathrm{d}P}{\mathrm{d}x} \tag{9}$$

No cavitation in recess

For the areas of the bearing containing parallel surfaces, the film thickness h is constant, and the pressure gradient must be linear (see Eq. 9). Equation (9) can be modified for each region of the bearing to

$$q_{AB} = \frac{U}{2}\frac{h_o^2+2\mu h_o\alpha_h}{h_o+\mu\alpha_h}-\frac{h_o^3}{12\mu}\frac{h_o+4\mu\alpha_h}{h_o+\mu\alpha_h}\left(\frac{P_2-P_{\text{atm}}}{a}\right) \tag{10}$$

$$q_{BC} = \frac{U}{2}\frac{h_p^2+2\mu h_p\alpha_h}{h_p+\mu\alpha_h}-\frac{h_p^3}{12\mu}\frac{h_p+4\mu\alpha_h}{h_p+\mu\alpha_h}\left(\frac{P_3-P_2}{b}\right) \tag{11}$$

$$q_{CD} = \frac{U}{2}\frac{h_o^2+2\mu h_o\alpha_h}{h_o+\mu\alpha_h}-\frac{h_o^3}{12\mu}\frac{h_o+4\mu\alpha_h}{h_o+\mu\alpha_h}\left(\frac{P_{\text{atm}}-P_3}{c}\right) \tag{12}$$

with one condition $q_{AB}=q_{BC}=q_{CD}$ based on volume conservation.

When q_{AB} is set to be equal to q_{CD}

$$\begin{aligned}&\frac{U}{2}\frac{h_o^2+2\mu h_o\alpha_h}{h_o+\mu\alpha_h}-\frac{h_o^3}{12\mu}\frac{h_o+4\mu\alpha_h}{h_o+\mu\alpha_h}\left(\frac{P_2-P_{\text{atm}}}{a}\right)\\&=\frac{U}{2}\frac{h_o^2+2\mu h_o\alpha_h}{h_o+\mu\alpha_h}-\frac{h_o^3}{12\mu}\frac{h_o+4\mu\alpha_h}{h_o+\mu\alpha_h}\left(\frac{P_{\text{atm}}-P_3}{c}\right)\end{aligned} \tag{13}$$

$$\left(\frac{P_2-P_{\text{atm}}}{a}\right)=\left(\frac{P_{\text{atm}}-P_3}{c}\right) \tag{14}$$

For the non-cavitating case, P_2 is unknown. Equating flow rate in inlet land and recess, $q_{AB}=q_{BC}$

$$\begin{aligned}&\frac{U}{2}\frac{h_o^2+2\mu h_o\alpha_h}{h_o+\mu\alpha_h}-\frac{h_o^3}{12\mu}\frac{h_o+4\mu\alpha_h}{h_o+\mu\alpha_h}\left(\frac{P_2-P_{\text{atm}}}{a}\right)\\&=\frac{U}{2}\frac{h_p^2+2\mu h_p\alpha_h}{h_p+\mu\alpha_h}-\frac{h_p^3}{12\mu}\frac{h_p+4\mu\alpha_h}{h_p+\mu\alpha_h}\left(\frac{P_3-P_2}{b}\right)\end{aligned} \tag{15}$$

If $K_o=\frac{\mu\alpha_h}{h_o+\mu\alpha_h}$ and $K_p=\frac{\mu\alpha_h}{h_p+\mu\alpha_h}$, then

$$\begin{aligned}&\frac{Uh_o}{2}(1+K_o)-\frac{h_o^3}{12\mu}(1+3K_o)\left(\frac{P_2-P_{\text{atm}}}{a}\right)\\&=\frac{Uh_p}{2}(1+K_p)-\frac{h_p^3}{12\mu}(1+3K_p)\left(\frac{P_3-P_2}{b}\right)\end{aligned} \tag{16}$$

From Eq. (14), it is known that $P_3=P_{\text{atm}}-\frac{c}{a}(P_2-P_{\text{atm}})$; therefore,

$$\left(\frac{P_3-P_2}{b}\right)=\frac{ab+bc}{ab^2}(P_{\text{atm}}-P_2) \tag{17}$$

Substitution of Eq. (14) in Eq. (15) gives

$$\begin{aligned}&P_2\left[\left(h_p^3+3h_p^3K_p\right)\frac{ab+bc}{ab^2}+\left(\frac{h_o^3+3h_o^3K_o}{a}\right)\right]\\&=P_{\text{atm}}\left[\left(h_p^3+3h_p^3K_p\right)\frac{ab+bc}{ab^2}+\left(\frac{h_o^3+3h_o^3K_o}{a}\right)\right]\\&\quad-6\mu U\left[\left(h_p+h_pK_p\right)-\left(h_o+K_o\right)\right]\end{aligned} \tag{18}$$

where

$$C_p^*=h_p^3+3h_p^3K_p$$
$$C_o^*=h_o^3+3h_o^3K_o$$
$$C_p=h_p+h_pK_p$$
$$C_o=h_o+h_oK_o$$

Combining Eqs. (17) and (18) to eliminate P_3 gives

$$P_2\left(\frac{ab+bc}{ab^2}C_p^*+\frac{C_o^*}{a}\right)=P_{\text{atm}}\left(\frac{ab+bc}{ab^2}C_p^*+\frac{C_o^*}{a}\right)-6\mu U\left(C_p-C_o\right) \tag{19}$$

and thus,

$$P_3=P_{\text{atm}}+\frac{6\mu U\left(C_p-C_o\right)bc}{aC_p^*+cC_p^*+bC_o^*} \tag{20}$$

Due to linearity between the pressure gradient in the inlet and outlet lands and in the recess, each of three areas of the bearing has a triangular pressure distribution that can be simply integrated to determine the load support. Therefore, the total normal force reads [21]:

$$W=W_{AB}+W_{BC}+W_{CD}-P_{\text{atm}}(a+b+c) \tag{21}$$

$$W=-\frac{6\mu U\left(C_p-C_o\right)ab}{aC_p^*+cC_p^*+bC_o^*}\left(\frac{a+b}{2}\right)+\frac{6\mu U\left(C_p-C_o\right)bc}{aC_p^*+cC_p^*+bC_o^*}\left(\frac{b+c}{2}\right) \tag{22}$$

Finally, the load support reads

$$W=\frac{6\mu U\left(C_p-C_o\right)}{C_p^*}\frac{b}{2}\left(\frac{c^2-ab-a^2+bc}{a+c+b\frac{C_o^*}{C_p^*}}\right) \tag{23}$$

Cavitation in recess

For the case of cavitation in recess, P_2 is assumed to be equal to P_{cav}, so $q_{AB}=q_{B'C}$ gives

$$\begin{aligned}&\frac{Uh_o}{2}\left(1+K_o\right)-\frac{h_o^3}{12\mu}\left(1+3K_o\right)\left(\frac{P_{\text{cav}}-P_{\text{atm}}}{a}\right)\\&=\frac{Uh_p}{2}\left(1+K_p\right)-\frac{h_p^3}{12\mu}\left(1+3K_p\right)\left(\frac{P_3-P_{\text{cav}}}{X_b}\right)\end{aligned} \tag{24}$$

where

$$X_b=\frac{C_p^*\left(P_3-P_{\text{cav}}\right)}{6\mu U\left(C_p-C_o\right)-C_o^*\left(\frac{P_{\text{atm}}-P_{\text{cav}}}{a}\right)} \tag{25}$$

It should be noted that for the cavitation zone, the pressure must be integrated separately, i.e. the non-cavitated area and cavitated area of the recess, so the total load support reads

$$W=W_{AB}+W_{BB'}+W_{B'C}+W_{CD}-P_{\text{atm}}(a+b+c) \tag{26}$$

Thus,

$$\begin{aligned}W=&\left[P_{\text{atm}}a+\frac{a^2}{2a}\left(P_{\text{cav}}-P_{\text{atm}}\right)\right]+\left[P_{\text{cav}}b\left(1-X_b\right)\right]\\&+\left[P_{\text{cav}}X_b+\frac{6\mu U\left(X_b\right)^2}{2C_p^*}\left(C_p-C_o\right)+\frac{C_o^*\left(X_b\right)^2}{2aC_p^*}\left(P_{\text{cav}}-P_{\text{atm}}\right)\right]\\&+\left[P_{\text{atm}}c-\frac{c^2}{2a}\left(P_{\text{cav}}-P_{\text{atm}}\right)\right]-P_{\text{atm}}(a+b+c)\end{aligned} \tag{27}$$

References

1. Safar ZS, Shawki GSA (1978) Do convective inertia forces affect turbulent bearing characteristics. Tribol Int 11(4):248–249
2. Kakoty SK, Majumdar BC (1999) Effect of fluid inertia on stability of flexibly supported oil journal bearings: linear perturbation analysis. Tribol Int 32:217–228
3. Khalil MF, Kassab SZ, Ismail AS (1992) Influence of inertia forces on the performance of turbulent externally pressurized bearings. Tribol Int 25(1):17–25
4. Stolarski TA, Chai W (2008) Inertia effect in squeeze film air contact. Tribol Int 41:716–723
5. Walicka A, Jurczak P (2017) Influence of total inertia effects in a thrust curvilinear bearing lubricated with Newtonian lubricants. Int J Appl Mech Eng 22(4):1045–1058
6. Okabe EP (2017) Analytical model of a tilting pad bearing including turbulence and fluid inertia effects. Tribol Int 114:245–256
7. Lin X, Jiang S, Zhang C, Liu X (2018) Thermohydrodynamic analysis of high-speed water-lubricated spiral groove thrust bearing considering effects of cavitation, inertia and turbulence. Tribol Int 119:645–658
8. Syed I, Sarangi M (2014) Hydrodynamic lubrication with deterministic micro textures considering fluid inertia effect. Tribol Int 69:30–38
9. Woloszynski T, Podsiadlo P, Stachowiak GW (2015) Evaluation of inertia effect in finite hydrodynamic bearings with surface texturing using spectral element solver. Tribol Int 91:170–176
10. Dobrica MB, Fillon M (2009) About the validity of Reynolds equation and inertia effects in textured sliders of infinite width. Proc Inst Mech Eng Part J J Eng Tribol 223:69–78
11. Salant RF, Fortier AE (2004) Numerical analysis of a slider bearing with a heterogeneous slip/no-slip surface. Tribol Trans 47:328–334
12. Wu CW, Ma GJ, Zhou P (2006) Low friction and high load support capacity of slider bearing with a mixed slip surface. J Tribol 128:904–907
13. Ma GJ, Wu CW, Zhou P (2007) Hydrodynamic of slip wedge and optimization of surface slip property. Sci China Phys Mech Astron 50:321–330
14. Ma GJ, Wu CW, Zhou P (2007) Influence of wall slip on the hydrodynamic behaviour of a two-dimensional slider bearing. Acta Mech Sin 23:655–661
15. Bayada G, Meurisse MH (2009) Impact of the cavitation model on the theoretical performance of heterogeneous slip/no-slip engineered contacts in hydrodynamic conditions. Proc Inst Mech Eng Part J J Eng Tribol 223:371–381
16. Rao TVVLN (2010) Analysis of single-grooved slider and journal bearing with partial slip surface. J Tribol 132:014501-1–014501-7
17. Aurelian F, Patrick M, Mohamed H (2011) Wall slip effects in (elasto) hydrodynamic journal bearing. Tribol Int 44:868–877
18. Tauviqirrahman M, Ismail R, Jamari J, Schipper DJ (2013) A study of surface texturing and boundary slip on improving the load support of lubricated parallel sliding contacts. Acta Mech 224:365–381

19. Syed I, Sarangi M (2018) Combined effects of fluid–solid interfacial slip and fluid inertia on the hydrodynamic performance of square shape textured parallel sliding contacts. J Braz Soc Mech Sci Eng 40:314
20. Wang L, Lu C (2015) Numerical analysis of spiral oil wedge sleeve bearing including cavitation and wall slip effect. Lubr Sci 27(3):193–207
21. Muchammad M, Tauviqirrahman M, Jamari J, Schipper DJ (2017) An analytical approach on the tribological behaviour of pocketed slider bearings with boundary slip including cavitation. Lubr Sci 29:133–152
22. Olver AV, Fowell MT, Spikes HA, Pegg IG (2006) 'Inlet suction' a load support mechanism in non-convergent pocketed hydrodynamic bearings. Proc Inst Mech Eng Part J J Eng Tribol 220:105–108
23. Fowell M, Olver AV, Gosman AD, Spikes HA, Pegg I (2007) Entrainment and inlet suction: two mechanisms of hydrodynamic lubrication in textured bearings. ASME J Tribol 129:337–347
24. ANSYS (2011) ANSYS Fluent, version 14.0: user manual. ANSYS Inc., Canonsburg
25. Dhande DY, Pande DW (2018) Multiphase flow analysis of hydrodynamic journal bearing using CFD coupled fluid structure interaction considering cavitation. J King Saud Univ Eng Sci 30:345–354
26. Sun D, Li S, Fei C, Ai Y, Liem RP (2019) Investigation of the effect of cavitation and journal whirl on static and dynamic characteristics of journal bearing. J Mech Sci Tech 33(1):77–86